European Journal of Soil Science

European Journal of Soil Science, 2015 doi: 10.1111/ejss.12269

Properties and bioavailability of particulate and mineral-associated organic matter in Arctic permafrost soils, Lower Kolyma Region, Russia

N. Gentsch[a], R. Mikutta[a], O. Shibistova[a,b], B. Wild[c,d,e], J. Schnecker[e,f], A. Richter[c,d], T. Urich[d,g], A. Gittel[h,i], H. Šantrůčková[j], J. Bárta[j], N. Lashchinskiy[k], C. W. Mueller[l], R. Fuß[m] & G. Guggenberger[a,b]

[a]*Institut für Bodenkunde, Leibniz Universität Hannover, Herrenhäuser Straße 2, 30419 Hannovern, Germany,* [b]*VN Sukachev Institute of Forest, Akademgorodok 50, 660036 Krasnoyarsk, Russia,* [c]*Division of Terrestrial Ecosystem Research, Department of Microbiology and Ecosystem Science, University of Vienna, Althanstr. 14, 1090 Vienna, Austria,* [d]*Austrian Polar Research Institute, Althanstraße 14, 1090 Vienna, Austria,* [e]*Department of Earth Sciences, University of Gothenburg, Guldhedsgatan 5A, 40530 Gothenburg, Sweden,* [f]*Department of Natural Resources and the Environment, University of New Hampshire, Durham, NH 03824, USA,* [g]*Department of Ecogenomics and Systems Biology, University of Vienna, Althanstr. 14, 1090 Vienna, Austria,* [h]*Department of Biology, Centre for Geobiology, University of Bergen, Postboks 7803, N-5020 Bergen, Norway,* [i]*Department of Bioscience, Norway and Center for Geomicrobiology, Aarhus University, Ny Munkegade 116, 8000 Aarhus C, Denmark,* [j]*Department of Ecosystem Biology, University of South Bohemia, Branisovska 1760, 37005 Ceske Budejovice, Czech Republic,* [k]*Central SiberianBotanical Garden, Siberian Branch of the Russian Academy of Sciences, Zolotodolinskya Street 101, 630090 Novosibirsk, Russia,* [l]*Lehrstuhl für Bodenkunde, Technische Universität München, Emil-Ramann Strasse 2, 85354 Freising, Germany , and* [m]*Thünen Institute of Climate Smart Agriculture, Bundesallee 50, D-38116 Braunschweig, Germany*

Summary

Permafrost degradation may cause strong feedbacks of arctic ecosystems to global warming, but this will depend on if, and to what extent, organic matter (OM) is protected against biodegradation by mechanisms other than freezing and anoxia. Here, we report on the amount, chemical composition and bioavailability of particulate (POM) and mineral-associated OM (MOM) in permafrost soils of the East Siberian Arctic. The average total organic carbon (OC) stock across all soils was 24.0 ± 6.7 kg m^{-2} within 100 cm soil depth. Density fractionation (density cut-off 1.6 g cm^{-3}) revealed that 54 ± 16% of the total soil OC and 64 ± 18% of OC in subsoil horizons was bound to minerals. As well as sorption of OM to clay-sized minerals ($R^2 = 0.80$; $P < 0.01$), co-precipitation of OM with hydrolyzable metals may also transfer carbon into the mineral-bound fraction. Carbon:nitrogen ratios, stable carbon and nitrogen isotopes, ^{13}C-NMR and X-ray photoelectron spectroscopy showed that OM is transformed in permafrost soils, which is a prerequisite for the formation of mineral-organic associations. Mineral-associated OM in deeper soil was enriched in ^{13}C and ^{15}N, and had narrow C:N and large alkyl C:(O-/N-alkyl C) ratios, indicating an advanced stage of decomposition. Despite being up to several thousands of years old, when incubated under favourable conditions (60% water-holding capacity, 15°C, adequate nutrients, 90 days), only 1.5–5% of the mineral-associated OC was released as CO_2. In the topsoils, POM had the largest mineralization but was even less bioavailable than the MOM in subsoil horizons. Our results suggest that the formation of mineral-organic associations acts as an important additional factor in the stabilization of OM in permafrost soils. Although the majority of MOM was not prone to decomposition under favourable conditions, mineral-organic associations host a readily accessible carbon fraction, which may actively participate in ecosystem carbon exchange.

Introduction

An increase in surface air temperatures, as already experienced during recent decades, facilitate permafrost thaw and promote active layer deepening, thermokarst formation, and river and coastal erosion (Fountain *et al.*, 2012). The most important consequences of climate change in permafrost environments are gradual or sometimes abrupt changes in the soil environmental conditions (such as thermal and moisture regime, and aeration) with direct consequences on organic carbon (OC) destabilization (Ping *et al.*, 2015). Long-term preserved OC will get increasingly exposed to microbial decomposition and be released from the active layer and the previously frozen ground to the atmosphere as CO_2 and

Correspondence: R. Mikutta. E-mail: mikutta@ifbk.uni-hannover.de

Received 7 July 2014; revised version accepted 12 March 2015

CH_4 (Nowinski *et al.*, 2010) or discharged by the drainage system (Vonk *et al.*, 2013). Warming of permafrost soils is also predicted to result in larger nutrient availability caused by new inputs of OC from shifting plant communities, increasing plant productivity and the spread of deep-rooting plant species (Hartley *et al.*, 2012). Under these conditions, priming reactions induced by the addition of fresh carbon sources might facilitate the release of older OC from subsoil horizons (Wild *et al.*, 2014). However, the magnitude of the processes stimulating OC loss from mineral soil horizons strongly depends on the soil parent material and the protective capabilities of the soil minerals.

Mineral-organic associations play a crucial role in soil organic matter (OM) preservation and mineral-associated OM (MOM) often accounts for the majority of total soil carbon (Kleber *et al.*, 2015). Variation in the mineral assemblage has been reported to not only to alter the OC contents and the composition of OM but also its bioavailability (Mikutta *et al.*, 2007). In this context, MOM is considered to be an amorphous structure of variable composition and bound to single or multiple mineral surfaces. In permafrost soils, the frequent moderately acidic to neutral pH (Alekseev *et al.*, 2003) and anoxic conditions, which induce the reduction of Fe(III) oxyhydroxides (Lipson *et al.*, 2012), might impair the stabilization of OM by Fe oxides in the subsoil. Despite the importance of OC preservation through mineral interactions, only a few studies have addressed the dynamics of MOM in high-latitude soils (Gundelwein *et al.*, 2007; Höfle *et al.*, 2013; Jagadamma *et al.*, 2013) and very little is known about the role of minerals in terms of their ability to sorb and stabilize OM.

Compared with OC that is attached to minerals, particulate OM (POM) from decaying plant material represents a more bioavailable carbon fraction (Schrumpf *et al.*, 2013). Such organic debris can accumulate close to the permafrost surface or within the permafrost as a consequence of cryoturbation (vertical soil mixing upon frequent freeze-thawing cycles) and is stabilized there over longer periods (Kaiser *et al.*, 2007). In contrast to the recognition that POM is more degradable than OM associated with minerals, Jagadamma *et al.* (2013) showed that, unlike for other soil types such as Andisols, Mollisols, Ultisols and Oxisols, MOM and POM from a Gelisol were decomposed at comparable rates during an incubation experiment and that MOM in the Gelisol tended to be respired faster than that from the other soils. Therefore, knowledge on the transformation of OM, its distribution in functional fractions across different soil horizons, and their potential decomposability, is important in order to assess the overall stabilization potential of OM in permafrost soils. Consequently, the main objectives of this study were to (i) investigate the soil mineralogical composition and quantify the OC portion associated with the mineral phase versus the OC proportion bound in POM, (ii) determine the degree of OM decomposition and (iii) test the potential bioavailability of MOM in comparison with POM. Organic matter fractions of permafrost soils were physically isolated by density separation and characterized for stable isotopes (^{13}C and ^{15}N), and their chemical composition was determined with solid-state ^{13}C nuclear magnetic resonance and X-ray photoelectron spectroscopy. Finally, both MOM and POM fractions were incubated for 90 days under optimal nutrient and temperature conditions to assess their potential bioavailability.

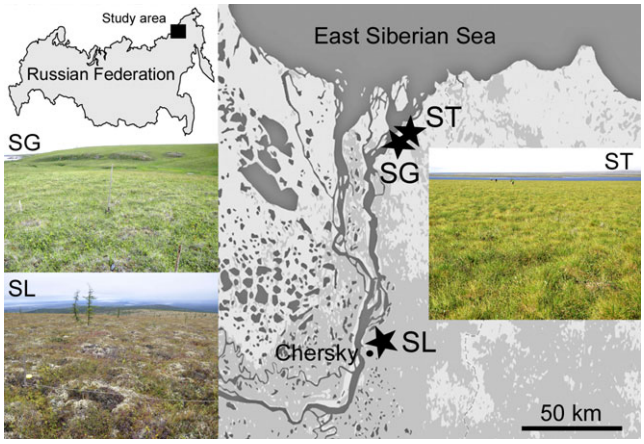

Figure 1 Study area and site locations of the different tundra types (SG, shrubby grass tundra; ST, shrubby tussock tundra; SL, shrubby lichen tundra) along the Kolyma River in east Siberia.

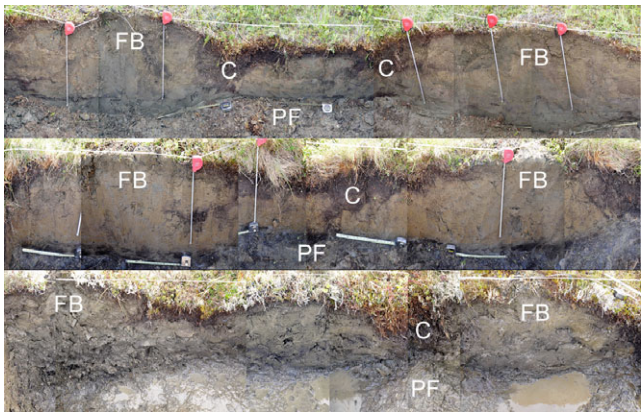

Figure 2 Profile images of selected Gelisol (Cryosol, WRB) pedons under shrubby grass (top), shrubby tussock (middle) and shrubby lichen (below) tundra vegetation. The width of the profiles is 5 m, the scale is 50 cm. FB, frostboil; C, crack; PF, permafrost table.

Materials and methods

Soil sampling and terminology

For this study we sampled three tundra ecosystems of northeastern Siberia along the lower Kolyma River, Russia (Figure 1): shrubby grass tundra (SG), shrubby tussock tundra (ST) and shrubby lichen tundra (SL). Detailed descriptions of the sites and sampling design are given in File S1 and Gentsch *et al.* (2015). Diagnostic horizons of three replicated 5-m soil trenches per tundra type were sampled (Figure 2), including two soil cores from the upper 45 cm of the permafrost. Bulk density (BD) samples from each horizon were taken in triplicate with 100-cm^3 stainless core cutters.

All soils showed strong signs of cryoturbation with hummock topography or bare frost boils being located adjacent to vegetated

depressions or cracks (Figure 2). Depressions had aquic moisture regimes and strong accumulation of OM. The soils were classified as Cryosols according to the IUSS Working Group WRB (2014) or Gelisols according to USDA Soil Taxonomy (Soil Survey Staff, 2010) (Table 1). Pockets of OM-enriched material (compared with topsoil materials) transferred into the subsoil by cryoturbation were sampled from several locations within the active layer; in the following these are referred to as 'subducted topsoil'. Living roots and macroscopic soil fauna were removed from all soil samples before they were dried and sieved to < 2 mm. The following terminology is used to summarize diagnostic soil horizons (symbols according to Soil Taxonomy): organic topsoil (O, Oa, Oe), mineral topsoil (A, AB), subducted topsoil (Ojj, Ajj) and subsoil horizons (BCg, Cg, Cff).

Soil characteristics

The texture composition was determined by the standard sieve-pipette method after removal of OM and Fe oxides (DIN ISO 11277, 2002). The effective cation exchange capacity (CEC_{eff}) was determined by extraction of soils with a Mehlich-3 solution (Ziadi & Tran, 2006); the extracted cations were measured by inductively coupled plasma optical emission spectroscopy (ICP-OES; Varian 725-ES, Varian Australia Pty Ltd, Mulgrave, Australia). The base saturation (BS) was calculated as percentage contribution of the basic cations (Ca, Mg, K and Na) to CEC_{eff}. Pedogenic Fe and Al fractions were determined by standard dithionite-citrate-bicarbonate (Fe_d) and acid oxalate extraction (Fe_o, Al_o) according to Pansu & Gautheyrou (2006). The Fe_d extract represents the amount of pedogenetically formed Fe within (hydr)oxides and silicates, as well as in organic complexes capable of acting as an electron acceptor, whereas Fe_o and Al_o originate from poorly crystalline aluminosilicates, ferrihydrite, Al-gels and Al- and Fe-organic complexes. Oxalate-soluble Fe also reflects the proportion of pedogenic Fe that dissolves in the initial stage of the dissimilatory Fe(III) reduction but may also contain some Fe extracted from biotite (Vodyanitskii *et al.*, 2008). The ratio Fe_o:Fe_d mirrors the portion of poorly crystalline Fe oxides to total pedogenic Fe oxides. Organically complexed Fe and Al (Fe_p, Al_p) were determined by extraction of mineral-organic associations by 0.1 M sodium-pyrophosphate solution adjusted to pH 9.0 and shaken for 16 hours. In order to avoid the dispersion of Fe and Al colloids, extracts were centrifuged at 300 000 ***g*** for 6 hours and Fe and Al in the supernatant liquid were measured by ICP-OES. Soil pH was measured in a soil-water suspension at a ratio of 1:2.5. The clay mineral composition of Fe-oxide and OM-free clay samples saturated with either K^+ (including heating to 550°C), Mg^{2+} or Mg^{2+}/glycol was determined by X-ray diffraction (Kristalloflex D500, Siemens AG, Mannheim, Germany) by CuKα radiation, at a step size of 0.05° and 10-s acquisition per time-step. Identification of the most abundant clay minerals was as outlined in section S1 of File S1.

Density fractionation, soil organic matter analyses and carbon storage

Density fractionation using sodium polytungstate (SPT; density cut-off 1.6 g cm^{-3}) was used to separate POM and MOM in mineral soil horizons. Because the investigated soils had a plastic consistency and little sign of aggregation, we did not isolate an aggregate-occluded POM fraction as is routine for non-permafrost soils. Twenty-five grams of soil were dispersed in 125 ml SPT for about 10 minutes with a total sonication energy of 60 J ml^{-1} using a LABSONIC® ultrasound homogenizer (Sartorius Stedim Biotech GmbH, Göttingen, Germany). The floating POM fraction was separated from the heavier MOM fraction by decantation after settling for 1 hour and centrifugation (3500 ***g***; for 10 minutes). Both fractions were washed with 18-MΩ water until the electrical conductivity was < 50 µS cm^{-1}, and freeze-dried. For samples with incomplete recovery of POM, the procedure was repeated without sonication until no POM remained floating. During the cleaning from SPT remnants, considerable amounts of OC and TN were mobilized from the MOM fraction. This mobilized fraction (MoF) was quantified by mass balance (Table 3) and may contain OM components that in soil might also easily move into the soil solution. Organic carbon and total nitrogen as well as the isotopic composition (^{13}C and ^{15}N) of fractionated and bulk samples were measured with an IsoPrime 100 IRMS (IsoPrime Ltd, Cheadle Hulme, UK) coupled to an Elementar vario MICRO cube (Elementar Analysensysteme GmbH, Hanau, Germany). Traces of carbonates ($< 0.5\%$) were removed by acid fumigation according to Harris *et al.* (2001) and subsequent neutralization was carried out over NaOH pellets (for 48 hours each). The $\delta^{13}C$ and $\delta^{15}N$ values of soil samples were corrected by calculating response factors determined by linear regressions between measured ^{13}C or ^{15}N contents and respective $\delta^{13}C$ or $\delta^{15}N$ values of standard compounds (for ^{13}C, sucrose, glutamic acid and caffeine; for ^{15}N, glutamic acid and caffeine, IAES $(NH_4)_2SO_4$ standards). The ^{13}C and ^{15}N values were expressed in the delta notation related to the Vienna Peedee-Belemnite-Standard (−20‰) and atmospheric N_2 (0‰), respectively. Dissolved OC (DOC) was quantified by extraction of soil with bi-distilled water (organic horizons 1:10 wt:vol; mineral horizons 1:20 wt:vol) for 2 hours. The filtered extracts (0.45 µm; MN-GF 5, MACHEREY-NAGEL, Düren, Germany) were analysed for DOC by a LiquiTOC analyser (Elementar Analysensysteme GmbH).

The radiocarbon content ($\Delta^{14}C$) of selected OM fractions was determined by accelerator mass spectrometry at the Klaus-Tschira-Laboratory for Radiometric Dating Methods at the Curt-Engelhorn-Centre for Archaeometry GmbH, Germany. Homogenized samples were pretreated by rinsing with 0.5 M HCl to remove traces of carbonates. The ^{14}C results were expressed in as a percentage of modern carbon (pMC), and conventional ^{14}C ages were calculated according to Stuiver & Polach (1977) and referenced to 1950 (1950 A.D. = 0 B.P).

Solid-state cross-polarization magic angle spinning ^{13}C-NMR analyses of ground OM fractions were made with a Bruker DSX 200 instrument (Bruker Biospin GmbH, Karlsruhe, Germany). Samples were filled into zirconium dioxide rotors and spun in a magic

Table 1 Site description, dominant plant species, morphological properties and soil taxonomic classification for three investigated tundra types

Land cover class	Site code/profile identifier	UTM	CAVM class/index	Dominant plant species	Active layer depth / cm	Soil classification (Soil Taxonomy)[a]	Soil classification (WRB)[b]
Shrubby grass tundra	SG/CH A-C	57W 0607781, 7706532	D/G3	*Betula exilis*, *Salix sphenophylla, Carex lugens*, *Calamagrostis holmii*, *Aulacomnium turgidum*	30–70	Ruptic-Histic Aquiturbel, fine silty	Histic Turbic Reductaquic Cryosol (Siltic)
Shrubby tussock tundra	ST/CH D-F	57W 0606201, 7705516	D/G4	*Eriophorum vaginatum*, *Carex lugens*, *Betula exilis*, *Salix pulchra.*, *Aulacomnium turgidum*	35–60	Ruptic-Histic Aquiturbel, clayey to fine silty	Histic Turbic Reductaquic Cryosol (Siltic)
Shrubby lichen tundra	SL/CH G-I	57W 0604930, 7628451	E/S2	*Betula exilis*, *Vaccinium uligonosum*, *Flavocetraria nivalis*, *Flavocetraria cucullata*	35–90	Typic Aquiturbel, fine silty to loamy-skeletal	Turbic Reductaquic Cryosol (Siltic)

[a]Soil Survey Staff (2010).
[b]IUSS Working Group WRB (2014).
CAVM denotes the Circum Arctic Vegetation Map according to Walker *et al.* (2005).

angle spinning probe at 6.8 kHz to minimize chemical anisotropy. A ramped 1H pulse was used during a contact time of 1 ms to prevent Hartmann–Hahn mismatches. The delay times ranged from 400 ms for MOM fractions to 1000 ms for POM fractions. Chemical shifts were referenced to tetramethylsilane (TMS = 0 ppm). Prior to analysis, the MOM fractions were treated with 10% hydrofluoric acid to remove mineral material, including paramagnetic compounds such as iron, and to concentrate OM (section S3, File S1). For integration, the following chemical shift regions were used: alkyl C (−10 to 45 ppm), O/N-alkyl C (45–110 ppm), aryl/olefine C (110–160 ppm) and carbonyl/carboxyl/amide C (160–220 ppm) (Höfle *et al.*, 2013).

X-ray photoelectron spectroscopy (XPS) was applied to nine MOM samples (the same number as used for ^{13}C-NMR) to study the composition of OM at the outermost mineral-organic interface (top ∼10 nm). The samples (< 63 µm) were deposited onto adhesive copper-nickel tape and analysed by a Kratos Axis Ultra DLD instrument (Kratos Analytical Ltd, Manchester, UK). The scans for survey spectra (pass energy, 160 eV; step size, 1 eV) and C1s detail spectra (pass energy, 10 eV; step size, 0.1 eV) were acquired in the hybrid lens mode with photoelectrons originating from an area of 300 × 700 µm. After charge correction, the C1s peak centered at 285 eV was de-convoluted into several sub-peaks representing different carbon oxidation states by least square fitting (Mikutta *et al.*, 2014). The following carbon types were distinguished according to Gerin *et al.* (2003): (i) carbon bound to hydrogen and carbon (C–C, C=C, C–H; at 285 ± 0.1 eV), (ii) carbon making a single bond to O or N as located in polysaccharides (C–O, C–N; at 286.5 ± 0.1 eV), (iii) carbon making two bonds to oxygen (C=O, O–C–O; at 287.9 ± 0.1 eV) and (iv) carbon making three bonds to O and N (O–C=O, O=C–N; at 289.3 ± 0.1 eV). For duplicate element quantification the error was typically < 5%; variation of duplicates for the different carbon species was on average 12%, with a median of 9%.

The OC stocks of the soils were quantified from the digitized 5-m^2 soil profiles by multiplying the area of a specific horizon with the bulk density and OC concentration (Gentsch *et al.*, 2015).

Incubation experiment

In order to test the potential bioavailability of OM fractions in comparison to the bulk soil in different soil horizons, 10 POM samples,18 MOM samples and 18 bulk soil samples were incubated in triplicate for 90 days at 60% water-holding capacity and 15°C in the dark. A Hoagland's solution provided all the necessary macro- (N, P, K, Ca, Mg and S) and micro-nutrients (Fe, Mn, Mo, B, Zn and Cu). We applied a purified quartz-silt mixture to ensure the same OC contents (50 mg total OC), substrate mass (20 g) and water-holding capacity in all treatments. Samples were inoculated with a solution containing 10^6 cells (determined by SYBR Green staining and fluorescence microscopy) extracted from a mixture of all 18 horizons (mineral top- and sub-soils, subducted topsoils and permafrost from all three tundra types). Previously, the microbial community in the soil mixture was reactivated with a 28-day incubation in the dark at 15°C and 60% water-holding capacity and thereafter extracted with 0.004 M $CaCl_2$ and filtered through 5–8-µm cellulose filters. After addition of the inoculum, the flasks were closed by polyethylene wool to allow for gas exchange with the atmosphere. Pre-equilibration of soil and OM fractions before the first gas sampling lasted for 7 days to avoid the rewetting-induced CO_2 pulse. Twenty-four hours before each gas sampling the flasks were closed and flushed with CO_2-free air. Gas samples were transferred to 20-ml pre-evacuated vials at days 0, 7, 14, 21, 28, 42, 56 and 90. Carbon dioxide emissions were measured with a GC equipped with an electron capture detector (Shimadzu GC 2014, Kyoto, Japan) and corrected for the CO_2 release from an inoculated quartz powder. Bulk soils were incubated analogously. Because of the similar mineralization rates of bulk OM

Table 2 Basic properties of the investigated soil pedons with respect to different tundra types (profile identifiers in parentheses are in accordance with Table 1)

		pH (H_2O)		Clay / %		Silt / %		Sand / %		Fe_d / mg g^{-1}		Fe_o / mg g^{-1}		Al_o / mg g^{-1}		Fe_p / mg g^{-1}		Al_p / mg g^{-1}		Fe_o:Fe_d		CEC_{eff} / $cmol_c$ kg^{-1}		BS / %	
Horizon	*N*	Mean	SD	Mean	SD	Mean	SD	Mean	SD	Mean	SD	Mean	SD	Mean	SD	Mean	SD	Mean	SD	Mean	SD	Mean	SD	Mean	SD
Shrubby grass tundra (A–C)																									
O	4	5.14	0.12	nd	nd	nd	nd	nd	nd	7.70	1.13	6.03	1.11	2.17	0.31	nd	nd	nd	nd	0.79	0.11	nd	nd	nd	nd
A	4	5.64	0.19	18.09	3.98	75.18	4.24	6.73	1.84	11.88	1.76	6.49	1.71	1.56	0.55	0.88	0.69	0.46	0.36	0.54	0.06	23.33	4.26	42.51	4.57
Ajj/Ojj	8	6.08	0.66	24.56	4.73	71.81	3.56	3.63	1.75	9.44	3.03	8.51	3.19	2.35	0.57	3.51	2.54	1.12	0.60	0.89	0.11	35.14	4.43	58.80	6.11
B/C	8	6.49	0.80	14.14	2.14	81.15	4.19	4.71	2.60	9.45	1.56	4.62	1.64	1.05	0.29	0.44	0.23	0.20	0.10	0.48	0.11	20.37	2.83	45.24	8.25
Cff	10	8.06	0.34	12.93	1.03	85.60	1.12	1.47	0.43	7.32	0.43	6.88	0.70	0.95	0.09	0.49	0.30	0.08	0.03	0.94	0.10	25.29	2.56	67.19	3.22
Shrubby tussock tundra (D–F)																									
O	6	5.28	0.12	nd	nd	nd	nd	nd	nd	8.93	3.29	7.80	2.98	2.83	0.77	nd	nd	nd	nd	0.88	0.10	nd	nd	nd	nd
A	4	5.49	0.34	22.14	5.25	71.24	3.89	6.62	1.46	12.43	1.93	7.82	1.36	1.85	0.80	0.63	0.11	0.40	0.05	0.64	0.17	23.99	3.82	39.87	3.24
Ajj/Ojj	6	5.34	0.13	36.66	11.13	59.46	9.35	3.88	2.42	19.87	5.16	19.09	6.49	3.19	0.32	7.09	2.94	1.63	0.35	0.95	0.15	30.31	1.49	46.14	5.71
B/C	9	5.64	0.16	20.18	0.86	73.21	1.51	6.61	1.10	10.52	3.15	9.45	1.73	1.44	0.14	1.39	0.79	0.35	0.04	0.89	0.30	21.84	0.74	36.18	2.56
Cff	12	6.68	0.82	20.11	4.89	72.63	6.80	7.27	2.53	11.27	2.62	7.09	3.03	1.20	0.34	0.90	0.59	0.21	0.09	0.68	0.32	23.61	1.36	52.56	5.65
Shrubby lichen tundra (G–I)																									
O	5	4.79	0.35	nd	nd	nd	nd	nd	nd	6.75	2.22	4.21	1.02	2.32	0.59	nd	nd	nd	nd	0.64	0.07	nd	nd	nd	nd
A	4	5.36	0.44	19.77	5.11	71.91	3.70	8.31	3.20	11.25	0.60	4.60	1.34	1.59	0.59	0.85	0.90	0.58	0.44	0.41	0.10	22.27	1.15	48.34	5.35
Ajj/Ojj	12	5.87	0.29	27.21	6.15	67.45	5.22	5.34	2.13	11.69	1.56	7.44	2.13	2.47	0.60	2.37	1.35	1.13	0.48	0.63	0.15	32.79	2.43	54.45	3.60
B/C	8	6.32	0.46	16.48	1.33	74.57	2.75	8.95	2.68	11.52	0.38	4.55	0.63	1.15	0.11	0.34	0.12	0.25	0.07	0.39	0.05	22.91	1.31	46.45	5.01
Cff	4	6.26	0.34	17.39	3.62	76.83	3.88	5.78	4.88	11.26	1.06	6.85	3.19	1.43	0.61	1.01	0.91	0.39	0.29	0.60	0.24	23.70	4.93	49.92	4.65

CEC_{eff}, effective cation exchange capacity; BS, base saturation; Fe_d, Fe extractable in dithionite-citrate-bicarbonate; Fe_o and Al_o, Fe and Al extractable in acid oxalate; Fe_p and Al_p, pyrophosphate-extractable Fe and Al, respectively; SD, standard deviation; nd, not determined.

compared with the density fractions, we can rule out toxic effects caused by tungsten residues (present at < 1 atom% on mineral surfaces based on XPS) during incubation of the MOM and POM. Averaged cumulative mineralization curves were most accurately described by a first-order decay model: $f = a \times \exp(-k\,t)$, where f is the remaining OC calculated from CO_2 loss (mg OC g^{-1} OC), a the fitted initial OC concentration scaled to one gram of OC, k the decomposition rate constant, and t the time. Note, the first-order decay model was applied to derive mineralization rates without underlying assumptions regarding the number of rate-limiting reactants or presence of multiple OC pools.

Statistics

Pearson correlation coefficients between soil, OM and incubation conditions, as well as regression analyses, were calculated with the software package SPSS Statistics vs. 21. If necessary, the data were log transformed to achieve a normal distribution. Differences between medians of properties were tested by the non-parametric Mann–Whitney *U*-test. Differences between soil horizons and incubation treatments were explored using analysis of variance (ANOVA), setting horizons and treatments as fixed or random effects, respectively. Significant differences within horizons or treatments were compared by the least significant difference (LSD) test. The figures 3 and 9 were produced with the R packages lattice and ggplot2.

Results and discussion

Mineral and organic matter properties

The soils had developed on late Pleistocene sediments and were all rich in silt (mean ± SD; 74 ± 8%; $N = 86$; Table 2), with smaller contributions of clay (21 ± 8%) and sand (6 ± 3%). Soil pH_{water} values ranged from 4.8 to 8.1, with smaller values in the organic and mineral topsoil horizons and larger ones in the mineral subsoils (Table 2). The CEC_{eff} of all analysed horizons ranged between 20 and 35 $cmol_c$ kg^{-1} and the base saturation varied from 36 to 67% (Table 2), implying that weathering of the tundra soils released considerable amounts of acidic cations (primarily Al), which were subsequently present in the exchange complex. Calcium and Mg^{2+} contributed on average 47 ± 9% to the exchange capacity: inclusion of Al^{3+} increased this portion to 94 ± 2%. Concentrations of total pedogenic soil Fe (Fe_d) were between 7 and 12 g kg^{-1} soil and similar to those reported in Vodyanitskii *et al.* (2008). A large proportion of Fe resided in forms capable of being reduced within a short time, such as ferrihydrite, as also indicated by average Fe_o:Fe_d ratios of between 0.39 and 0.95. Organically complexed Fe and Al were more enriched in subducted topsoil horizons (Fe_p, 2.3–7.1 g kg^{-1}; Al_p, 1.1–1.6 g kg^{-1}; Table 2) than in adjacent subsoil horizons (Fe_p, < 1.5 g kg^{-1}; Al_p, < 0.6 g kg^{-1}). The X-ray diffraction of clay fractions from selected soil horizons revealed a fairly homogeneous clay mineral assemblage dominated by disordered, expandable interstratified minerals (1.4–1.7 nm), vermiculite, chlorite, illite and kaolinite (Figure 3; Figure S1, File S1). The minor variation of clay minerals in the different tundra soil horizons might indicative a homogeneous aeolian parent material or the mixing of soil material by cryoturbation ('cryo-homogenization'). While kaolinite is of detrital origin, the slight change from illite towards vermiculite in topsoils (Figure 3) reflects abundant but slow chemical weathering in these high-latitude soils (Borden *et al.*, 2010).

Average OC concentrations in the soils were largest in the organic topsoil, followed by the subducted topsoil horizons (Ajj/Ojj) where

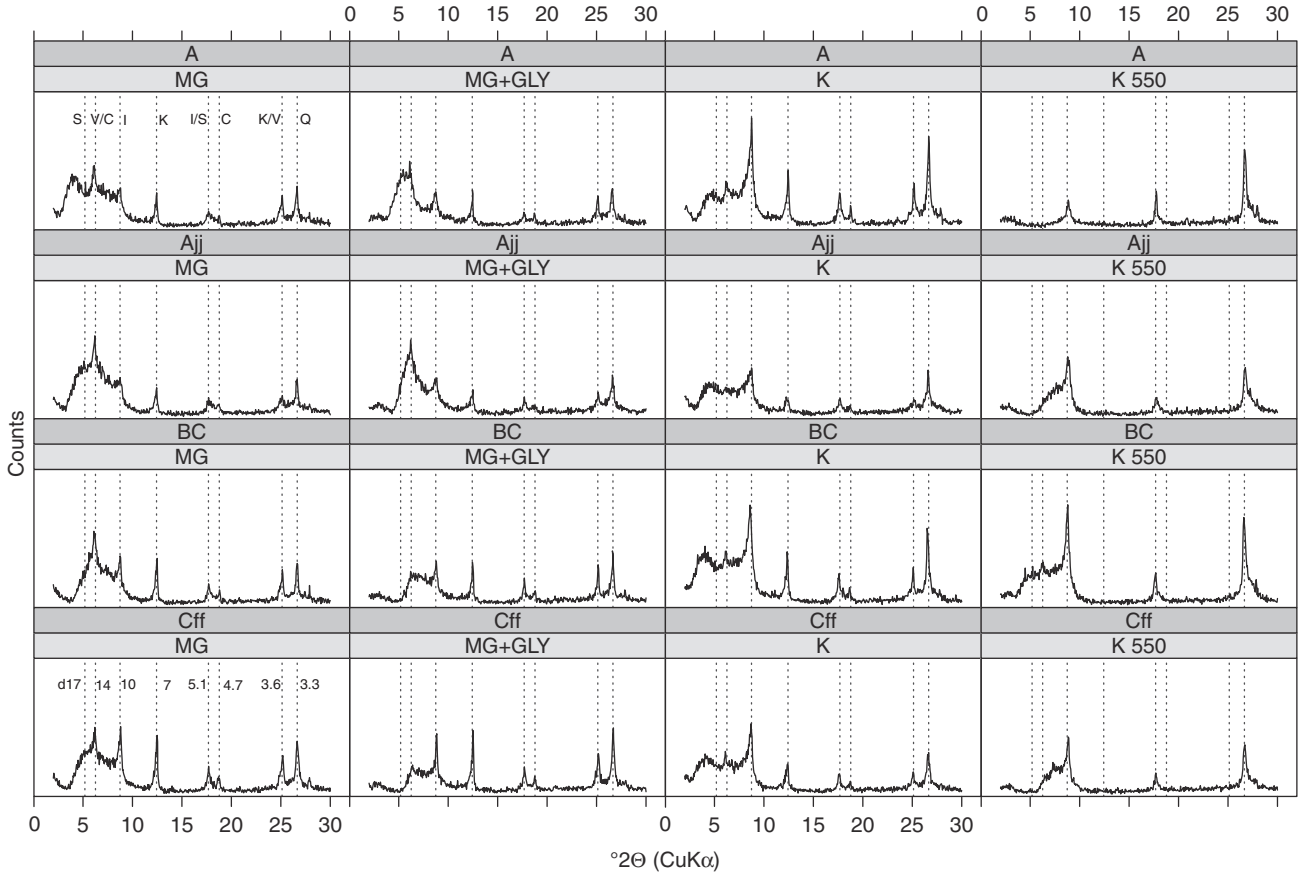

Figure 3 X-ray diffractograms of clay fractions from one soil profile under shrubby grass tundra vegetation. Diffractograms of clays from all tundra sites are provided in File S1. Diagnostic soil horizons and clay sample treatment (MG, Mg^{2+}; MG + GLY, Mg^{2+}/glycol; K, K^{+}; K 550, K^{+}/heating to 550°C) are given in the heading. S, smectite; V, vermiculite; C, chlorite; K, kaolinite; I, illite (Mica); Q, quartz. The d-scale is given in Ångstroms.

average values for the three tundra types ranged between 68 and 155 mg OC g^{-1} soil, and smallest in the mineral subsoil (BCgjj and Cgjj) and permafrost (Cff) horizons (Schnecker *et al.*, 2014). Total OC stocks of the soils ranged between 15 and 33 kg m^{-2} OC (average 24 ± 6 kg m^{-2}) within the upper 100 cm, with only slight differences among the tundra types (Gentsch *et al.*, 2015; Table S1, File S1). When considering all soil pedons ($N = 9$), 36 ± 20% of the total OC stocks were in the upper permafrost, while 20 ± 12 and 13 ± 4% were stored in topsoil (O and A) and subducted topsoil horizons (Ojj and Ajj), respectively. The large stock of 19 ± 6 kg m^{-2} OC in subsoil horizons (82 ± 27% of the total OC) highlights the relevance of subsoil environments for storing large quantities of OM.

Density fractions and mineralogical controls on carbon accumulation

Density fractionation revealed that 19 ± 10% of the bulk OC in mineral soil horizons was present as POM. The largest proportion of POM-C was found in subducted topsoils as well as permafrost horizons (Table 3). The fraction of OC bound to minerals (MOM) accounted for 62 ± 13% of the bulk OC, with no significant differences between the soil horizon classes (ANOVA; Table S2, File S1; mean values Table 3). Despite the good recovery of soil mass (96 ± 2%), 19 ± 14% of the total OC was mobilized during density fractionation, with the smallest proportions in subducted topsoil horizons (8 ± 4%). Whereas 2–13% (0.1–0.4 mg g^{-1}) of the MoF can be attributed to initial DOC in mineral horizons (Table 3), most of it results from the SPT-induced desorption of OM from mineral-organic associations (Gentsch *et al.*, 2015). Nevertheless, the MOM fraction was the dominant OC pool, holding 54 ± 16% of OC in the upper 100 cm of the pedon, with an even larger share (64 ± 18%) in subsoil horizons (Table S1, File S1).

Mineral-associated OC was strongly related to the clay content ($R^2 = 0.80$; $P < 0.01$) and Al_o concentrations ($R^2 = 0.82$; $P < 0.01$), as well as to Fe_p and Al_p concentrations ($R^2 = 0.90$ and 0.91, respectively; $P < 0.001$). Weaker linear relationships were observed with Fe_d ($R^2 = 0.37$; $P < 0.01$) and Fe_o concentrations ($R^2 = 0.60$; $P < 0.01$). Figure 4 shows that across all pedons the molar concentration of mineral-associated OC plotted against those of $Fe_p + Al_p$ is a straight line with a slope of 0.0181 ± 0.0004 ($N = 85$), which translates into an overall molar (Fe + Al):C ratio of 0.02. This result suggests that MOM in the tundra soils is 'proportionally' loaded with Fe and Al depending on the amount of OM present,

Table 3 Organic C and TN concentrations of the bulk soil and OM fractions received from density fractionation

			OC / mg g^{-1}								TN / mg g^{-1}								DOC / mg g^{-1}	
			Bulk		POM		MOM		MoF		Bulk		POM		MOM		MoF		Bulk	
Horizon	*N* Bulk	*N* Fractions	Mean	SD	Mean	SD	Mean	SD	Mean	SD	Mean	SD	Mean	SD	Mean	SD	Mean	SD	Mean	SD
Shrubby grass tundra																				
O	4	nd	206.10	49.39	nd	nd	nd	nd	nd	nd	9.35	1.03	nd	nd	nd	nd	nd	nd	1.42	0.89
A	4	4	28.10	29.46	5.29	5.25	17.65	19.85	5.17	4.59	2.05	1.88	0.18	0.20	1.48	1.29	0.52	0.47	0.23	0.14
Ajj/Ojj	8	8	109.87	61.62	48.68	62.20	55.39	19.45	5.79	2.28	6.44	2.58	2.06	2.59	5.05	2.25	0.30	0.17	0.41	0.12
B/C	8	8	10.42	2.53	1.67	0.57	6.80	1.39	1.95	1.66	0.95	0.15	0.06	0.03	1.23	1.11	0.22	0.19	0.08	0.03
Cff	10	10	8.98	1.88	1.90	0.94	5.22	1.15	1.86	1.10	0.96	0.12	0.11	0.06	2.30	2.21	0.19	0.13	0.16	0.08
Shrubby tussock tundra																				
O	6	nd	262.58	68.12	nd	nd	nd	nd	nd	nd	11.42	1.80	nd	nd	nd	nd	nd	nd	1.82	0.95
A	4	3	47.24	51.21	5.74	1.18	12.82	4.47	3.12	2.06	2.84	2.96	0.15	0.05	1.04	0.27	0.28	0.01	0.42	0.19
Ajj/Ojj	6	5	154.87	43.44	62.92	17.96	101.52	27.82	5.87	3.18	8.36	2.29	2.51	0.79	6.11	1.75	0.46	0.27	0.44	0.15
B/C	9	9	16.57	4.97	1.96	0.81	11.62	4.47	3.47	2.21	1.28	0.28	0.05	0.03	0.98	0.26	0.28	0.18	0.10	0.04
Cff	12	11	25.64	24.55	3.07	2.28	11.76	7.11	9.15	21.15	1.64	0.84	0.12	0.11	1.05	0.39	0.36	0.44	0.24	0.15
Shrubby lichen tundra																				
O	5	nd	257.15	74.38	nd	nd	nd	nd	nd	nd	10.12	2.34	nd	nd	nd	nd	nd	nd	2.30	1.50
A	4	4	51.74	54.85	9.76	6.74	30.88	25.59	19.29	20.87	2.33	1.53	0.28	0.22	2.07	1.62	0.38	0.16	0.62	0.58
Ajj/Ojj	12	10	67.59	31.82	12.10	6.56	55.81	22.72	8.80	4.42	4.54	2.04	0.45	0.25	4.06	1.48	0.71	0.42	0.44	0.24
B/C	8	8	12.02	5.98	1.07	0.31	6.08	1.74	4.86	5.66	1.06	0.26	0.04	0.01	0.69	0.13	0.33	0.20	0.08	0.02
Cff	4	4	28.92	26.35	4.98	5.28	17.75	19.32	6.19	1.91	2.05	1.57	0.19	0.23	1.45	1.29	0.41	0.07	0.65	1.07
All land-cover classes combined[a]																				
O	15	nd	245.71	66.16	nd	nd	nd	nd	nd	nd	10.43	1.94	nd	nd	nd	nd	nd	nd	1.90	0.29
A	12	11	42.36	43.44	7.04	5.18	21.14	19.55	8.79	12.57	2.41	2.03	0.21	0.17	1.57	1.22	0.41	0.30	0.42	0.11
Ajj/Ojj	26	23	100.74	56.07	35.87	42.31	66.05	29.29	7.24	3.73	6.01	2.68	1.46	1.77	4.88	1.94	0.55	0.38	0.43	0.04
B/C	25	25	13.15	5.27	1.58	0.69	8.30	3.83	3.43	3.68	1.11	0.27	0.05	0.03	0.97	0.66	0.29	0.19	0.09	0.01
Cff	26	25	19.74	20.65	2.90	2.67	10.10	9.44	5.62	13.70	1.44	0.88	0.13	0.12	1.61	1.56	0.33	0.34	0.28	0.09

[a]Published in Gentsch *et al.* (2015).

DOC, dissolved OC; POM, particulate organic matter; MOM, mineral-associated organic matter; MoF, mobilizable fraction; SD, standard deviation; *N*, sample number; nd, not determined.

irrespective of the soil horizon considered. A linear regression between the moles of $Fe_p + Al_p$ and the mass of MOM (OC-OM conversion factor, 1.7) results in a slope of $9 \times 10^{-4} \pm 2 \times 10^{-5}$ mol $[Fe_p + Al_p]$ g^{-1} OM, which is in the reported range of Fe concentrations that can be complexed by humic substances at pH 5–7 (10^{-3} to 10^{-4} mol g^{-1}; Tipping *et al.*, 2002). These estimates show that under the arctic conditions sufficient mineral weathering must take place to produce dissolved Fe and Al concentrations large enough to saturate the remaining available binding sites of the MOM. Moreover, the molar $(Fe_p + Al_p)$:C ratio of 0.02 is close to the metal:C ratio of 0.03–0.05 at which significant precipitation of metal-organic complexes has been reported (see review by Kleber *et al.*, 2015). Therefore, apart from adsorption of DOC onto mineral surfaces, another conceivable pathway in the formation of mineral-organic associations in permafrost soils involves the formation of Fe and Al co-precipitates, which represent variable mixtures of insoluble metal-organic complexes and poorly ordered mineral phases (Kleber *et al.*, 2015).

As a result of the temporal anoxic conditions in the Kolyma lowland soils and the reductive dissolution of Fe(III) oxides and Fe(III) in phyllosilicates (Vodyanitskii *et al.*, 2008), Fe^{2+}_{aq} accumulates in the active layer as the permafrost table impedes drainage (Alekseev *et al.*, 2003). Upon aeration, Fe^{2+} becomes re-oxidized to Fe^{3+} and precipitates with dissolved OM as either Fe-organic complexes and

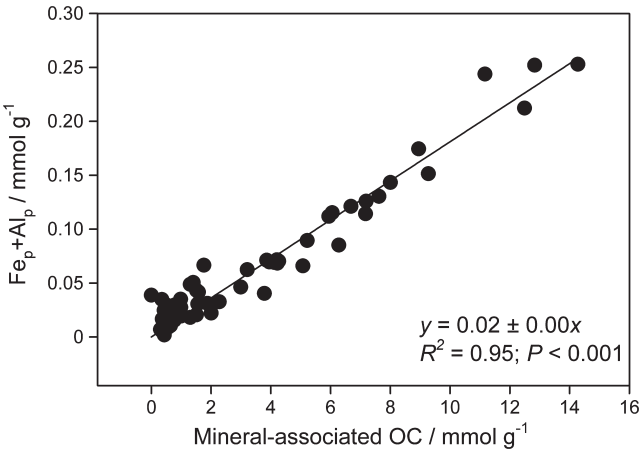

Figure 4 Relationship between the sum of pyrophosphate-extractable Fe and Al concentrations $(Fe_p + Al_p)$ and the amount of mineral-associated OC in mineral horizons of the nine soil profiles. The errors of the linear regression were tested for normality by a Q–Q plot.

or organically loaded Fe oxides such as poorly crystalline Fe phases, ferrihydrite or lepidocrocite (the latter was described by Alekseev *et al.*, 2003). The annual freezing in the active layer also forms segregation ice while increasing the absolute solute concentrations in

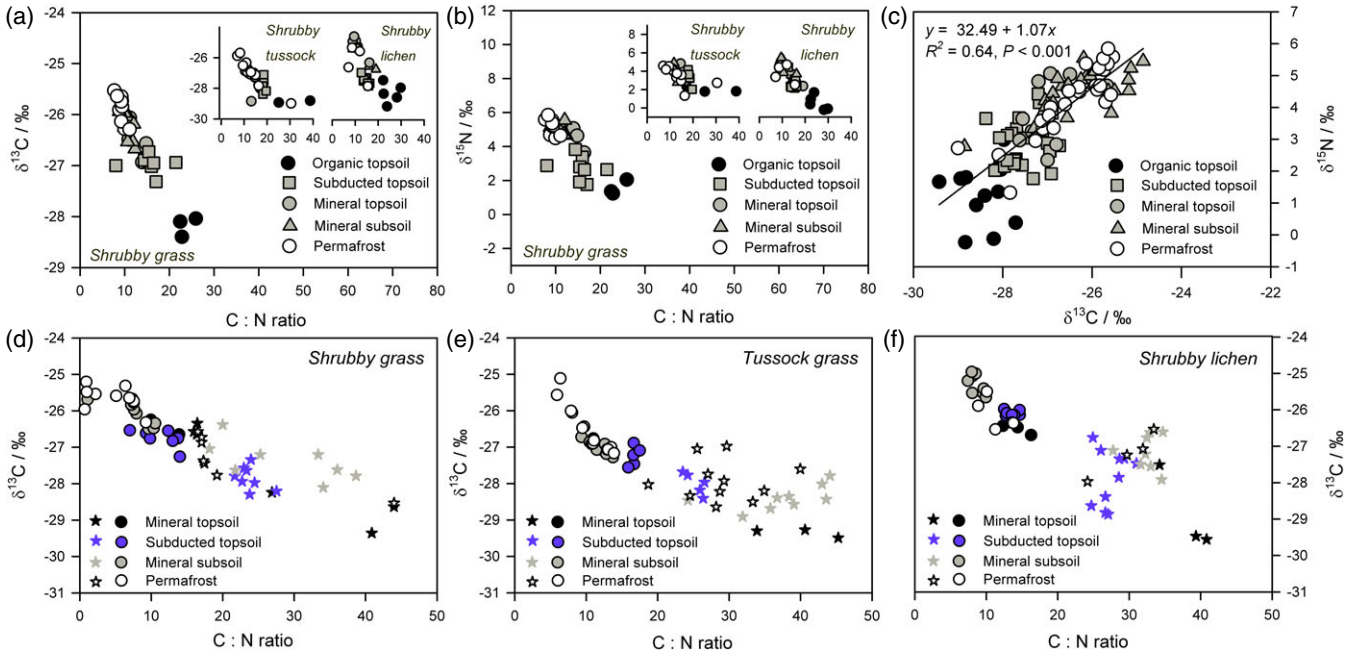

Figure 5 Bulk soil relationships between (a) δ^{13}C and C:N ratios and (b) δ^{15}N and C:N ratios, as well as between (c) the δ^{13}C and δ^{15}N isotopic ratios across all examined pedons. (d–f) Show the relationship between the δ^{13}C and C:N ratio of mineral-associated (cycles) and particulate OM (stars) under different tundra vegetation. Note, C:N ratios below about five as observed for some samples at the shrubby grass tundra site (d) imply a contribution from inorganic N.

the pore water. Thus, DOC, Fe and Al concentrations can be such that they flocculate or co-precipitate (Ostroumov, 2004). Overall, our data provide evidence that most of the OM in mineral horizons exists in association with clay-sized minerals (mainly phyllosilicates and poorly ordered Fe and Al phases), while the cryohydromorphic soil conditions are able to promote the formation of co-precipitates from OM and hydrolyzable metals. The large contribution of exchangeable multivalent metals and the moderately acidic conditions further suggest that the clay minerals primarily hold OM through the formation of cation bridges (Mikutta *et al.*, 2007).

Isotopic composition of bulk organic matter and density fractions

There was a general decrease in the C:N ratio of bulk OM from organic layers to topsoil mineral horizons, subsoil horizons and to the permafrost (Figure 5; Schnecker *et al.*, 2014), indicating a preferential loss of carbon relative to nitrogen. The decline of C:N ratios was accompanied by an enrichment of both ^{13}C and ^{15}N (Figure 5a, b), suggesting an on-going decomposition and subsequent enrichment of isotopically heavy microbial products with soil depth. Likewise, Nadelhoffer *et al.* (1996) observed a 2–5‰ increase in δ^{15}N within the top 20–30 cm of moist sedge and tussock tundra soils in Alaska. When examining the MOM and POM fractions individually, the linear relationships between the C:N ratios and δ^{13}C values persisted but the POM consistently had more scatter than the MOM (Figure 5d–f). Combining all bulk samples (including organic layers and mineral horizons; $N = 100$) demonstrated a significant linear relationship between δ^{13}C and δ^{15}N with a slope of 1.07 ± 0.08 (Figure 5c), suggesting that in the tundra soils studied, C and N transformation processes are tightly coupled. Although N losses from permafrost-affected soils are negligible because of poor drainage and efficient N cycling, N transformation processes (ammonification, nitrification and denitrification) occur at slow rates (Wild *et al.*, 2013), which is also indicated by the presence of $[NO_3 + NH_4]$-N in our soils (data not shown). Because nitrification, denitrification and enzymatic hydrolysis discriminate against ^{15}N by the preferential use of ^{14}N, the residual OM will become enriched in ^{15}N. Mycorrhizal activity might also cause N isotope fractionation, but as fungal biomass at the study sites declines with soil depth (Gittel *et al.*, 2014), fungal activity cannot explain the increase in ^{15}N with soil depth. Therefore, it is more reasonable to assume that the declining dilution with isotopically lighter POM, as well as the slow but persistent OM transformation over time, caused the enrichment of ^{13}C and ^{15}N in older OM at greater depth (^{14}C data see Figure 6). As the δ^{13}C values of MOM were significantly larger and C:N ratios smaller ($P < 0.001$; $N = 84$) than for POM, microbial-derived ^{13}C- and N-enriched compounds provide an important source for the formation of MOM.

Two soil profiles were investigated for ^{14}C activities of OM density fractions. The MOM had mean ^{14}C activities ranging from 88.0 pMC (1060 years BP) to 34.9 pMC (8410 years BP) and was 150–3000 years older than the respective POM (Figure 6). Although the soils are characterized by cryogenic activity, the ^{14}C activity of the MOM declined conventionally with soil depth.

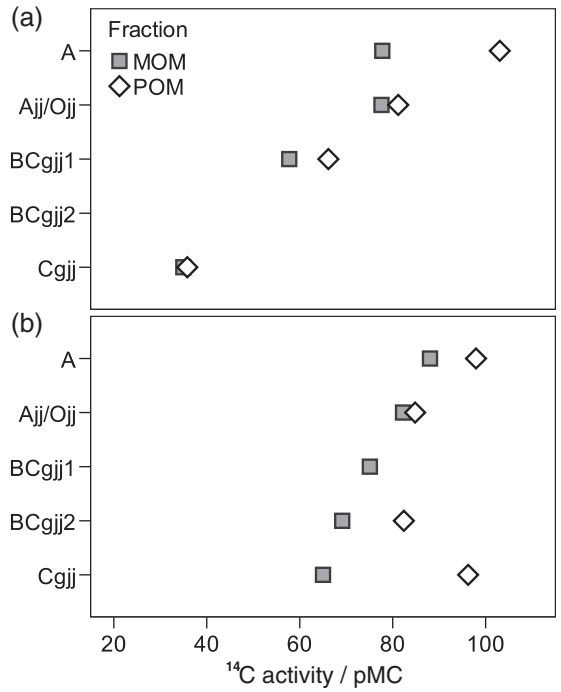

Figure 6 ^{14}C activity of mineral-associated (MOM) and particulate OM (POM) in two soil profiles (profile A (a) and D (b); Table 1) under shrubby grass and tussock grass vegetation as an approximate function of soil depth. Analytical errors are smaller than the symbols; one POM fraction in the lower panel could not be measured because of insufficient amounts.

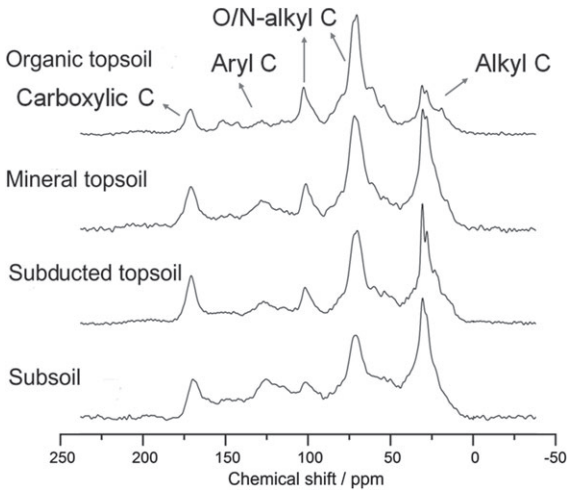

Figure 7 Chemical composition of the organic layer and MOM fractions in a shrubby grass tundra pedon as revealed by solid-state ^{13}C-NMR spectroscopy. The following chemical shift regions were used: alkyl C (−10 to 45 ppm), O/N-alkyl C (45–110 ppm), aryl/olefine C (110–160 ppm) and carbonyl/carboxyl/amide C (160–220 ppm). All NMR data are summarized in Table S3 of File S1.

The presence of younger POM (309 years BP) in the deep Cgjj horizon (Figure 6, lower panel) resulted from its incorporation from adjacent subducted topsoil pockets. This suggests that cryogenic mass exchange transfers younger POM to the subsoil while 'fresh' dissolved OM appears not to be leached directly from topsoil into the subsoil, which would have caused a rejuvenation of the subsoil MOM. The existing difference in ^{14}C activity between POM and MOM in most horizons, however, mirrors the stabilization of OM by the formation of mineral-organic associations.

Chemical composition of OM fractions

The ^{13}C-NMR spectroscopy showed that in comparison with organic soil layers, both MOM and POM were depleted in O-/N-alkyl C but enriched in aryl C (Table S3, File S1). Nevertheless, O-/N-alkyl C as contained in polysaccharides constituted the dominant fraction of MOM, followed by alkyl C and aryl C (Figure 7). Compared with POM, the MOM fraction was slightly but significantly depleted in aryl C ($P = 0.024$; $N = 9$) but tended to contain more O-/N-alkyl C ($44 \pm 3\%$), alkyl structures ($30 \pm 5\%$) and carboxyl/amide C ($9 \pm 5\%$).

An increasing transformation of OM with soil depth was reflected by the increasing alkyl C:(O-/N-alkyl C) ratio in POM and MOM in all observed profiles (Table S3, File S1). Together with the narrower C:N ratios and the $^{13}C/^{15}N$ enrichment with soil depth this also reflects the ongoing degradation of the POM and contribution of microbial products to the MOM, such as cell wall remains and lysis products or extracellular polymeric substances. The ratio of O-alkyl C as derived from C2, C3 and C5 signals of carbohydrates (70–75 ppm) to the methoxyl C signal of lignin (52–57 ppm) serves as another indirect proxy of OM decomposition (Bonanomi *et al.*, 2013). The increase of the (70–75 ppm):(52–57 ppm) ratio with soil depth (Table S3, File S1) suggests that in comparison to the organic layers, both POM and MOM were depleted in carbohydrates, implying a preferential degradation of carbohydrates once OM enters the mineral soil, while lignin is selectively preserved. Under anaerobic conditions lignin is apparently not biodegradable by fungi or lignin-decomposing *Actinobacteria* and other bacteria present in permafrost soil (Gittel *et al.*, 2014) and requires at least temporarily oxic conditions. Gittel *et al.* (2014), however, identified some anaerobic lignin-degrading bacteria in the study soils but their activity is presumably slow. The greater proportion of aryl components in MOM than in the organic topsoil can, in addition to biological processes, be explained by the retention of lignin-containing DOC, which forms stronger surface complexes with minerals than hydrophilic OM rich in carbohydrates and is more readily precipitated (Kleber *et al.*, 2015). Höfle *et al.* (2013) also found in clay fractions from a tundra Gelisol that aryl components became more enriched in progressively older OM with increasing soil depth (0–30 cm) than carbohydrates.

We applied XPS as a complementary, non-destructive method, yielding information about carbon oxidation states at the outermost particle surfaces. Carbon 1 s spectra (Figure 8) showed that the outermost MOM was composed of carbons primarily bonded in aliphatic and aromatic structures (type-I carbon; at 285 ± 0.1 eV; $52 \pm 8\%$; $N = 9$), followed by O–C (and N–C carbons) mainly located in polysaccharides (type-II carbon; at

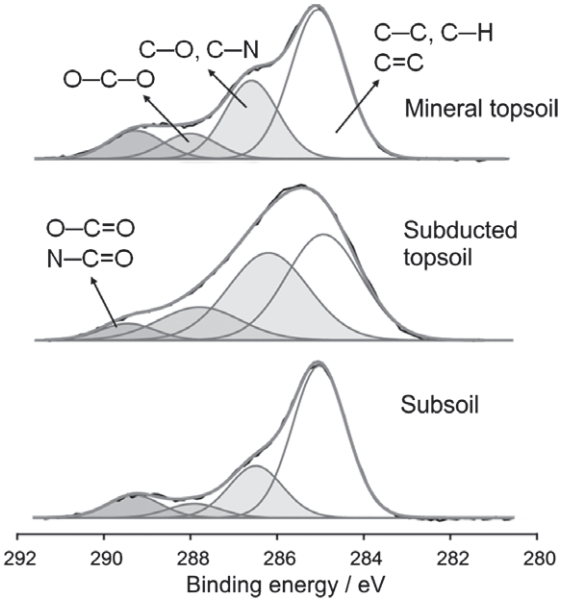

Figure 8 The XPS C1s spectra from the MOM fraction in a shrubby grass tundra pedon. Spectra are arranged from the top down with increasing soil depth and include the fitted carbon sub-components, the sum curve and the underlying measured spectrum (black line). The following carbon species were distinguished (all sample data summarized in Table S4, File S1): aliphatic and aromatic carbon (C–C, C=C, C–H), carbon making a single bond to O (or N) as located primarily in polysaccharides (C–O, C–N), carbon making two bonds to oxygen (C=O, O–C–O), and carbon making three bonds to O and N (O–C=O, O=C–N) as present in carboxylic acids and proteins.

286.5 ± 0.1 eV; 29 ± 5%). Carboxyl and amide carbons constituted about 8 ± 2% of total C (Table S4, File S1). Particles in subducted topsoil horizons contained more type-II carbons than those in either adjacent topsoil or subsoil horizons, suggesting that polysaccharides were more effectively protected against biodegradation in the subducted topsoils. The ratio of the type-(I) and type-(II) carbons indicated a similar trend to that observed for the NMR-based degradation ratios, with less oxidized carbon forms (aromatic and aliphatic C) increasing in deeper soil horizons (Table S4, File S1). All chemical characteristics, therefore, suggest that mineral-organic associations in the deep active layer contain a larger portion of microbial-derived OM, which agrees with the declining C:N ratios and increasing δ^{13}C and δ^{15}N bulk values with soil depth.

Potential bioavailability of organic matter fractions

Density fractionation generally affects the integrity of a given sample as it disperses soil particles, and thereby potentially enhances the spatial accessibility of OM for microbes, and causes loss of OC (MoF; Table 3). Because minerals stabilize OM by formation of chemical bonds between functional groups and the mineral surface (Kleber *et al.*, 2015), OM recovered as MOM must, therefore, be held by stronger bonds than the MoF. Hence, we can test the potential bioavailability of the OM associated with minerals by using the > 1.6-g cm^{-3} soil fraction in an incubation experiment. When the different OM fractions, spanning a wide range of chemical compositions and ^{14}C ages, were exposed to an active microbial community at 15°C (approximately the maximum topsoil temperature in the study area) for 90 days under optimal nutrient conditions, roughly 1.5–5% of the initial OC was mineralized. The total mineralization was significantly larger in mineral topsoil horizons than in any of the subsoil horizons (ANOVA [1], Tables S5 and S6, File S1). Because of minor deviations in the subsoil respiration, topsoil (AB, Figure 9) and subsoil horizons (Ajj, BCg and Cg/Cff, Figure 9) were clustered as two independent subsets. In topsoil horizons, the largest OC mineralization was with the POM fraction (4.4 ± 0.7%), followed by the bulk soil (3.8 ± 1.0%) and MOM fraction (3.1 ± 0.6%), although these differences were not statistically significant (ANOVA [2], Tables S5 and S6, File S1). In contrast, significant differences between treatments were observed in the subsoil (ANOVA [3], Tables S5 and S6, File S1), with the most mineralization occurring for the MOM fraction, followed by POM and bulk soil (2.5 ± 0.5, 1.9 ± 0.4 and 1.6 ± 0.2%).

The amount of respired carbon corresponds well with the fast cycling OM fraction as judged from a meta-analysis of long-term incubation data of circum-arctic soils (Schädel *et al.*, 2013) and was also comparable to recent results reported for a 98-day biodegradation experiment with mineral soil horizons from Canadian Cryosols (Gillespie *et al.*, 2014). We observed a respiration pulse from the bulk soil at the beginning of the experiment that can be assigned to an easily available OM fraction that was removed from the OM fractions during density fractionation. This large initial CO_2 flush reflects the greater bioavailability of the MoF. However, given that the bulk soils still contained the MoF-OC but the overall extent of OC mineralization was even less than that of the OM fractions, the carbon lost during the density fractionation either was not significantly more bioavailable than the remaining OM or it was well stabilized by the mineral phase and only became mobilized upon addition of SPT. The fit of a first-order decay model to CO_2 emission data showed equally valid results statistically as those for the total mineralization (Figure 10). The POM fractions had the largest mineralization rates compared with MOM and bulk material in the topsoil (ANOVA [4], Tables S5 and S6, File S1), while the LSD test (ANOVA [5], Tables S5 and S6, File S1) indicated significant differences between all treatments in the subsoil, with the fastest rates for the MOM fraction, followed by POM and the bulk soil. The NMR-based O-alkyl C:methoxyl C ratio of the MOM fractions was related to the mineralization rate constant ($R^2 = 0.37$; $P < 0.05$; $N = 9$) and suggests that MOM rich in carbohydrates (topsoil horizons) decomposed faster than that containing more lignin compounds in the subsoil.

Implications of the incubation experiment and controlling factors

Despite the larger accessibility of OM and the optimal temperature and nutrient conditions in this experiment, the MOM largely resisted microbial decomposition. The total amount of respired

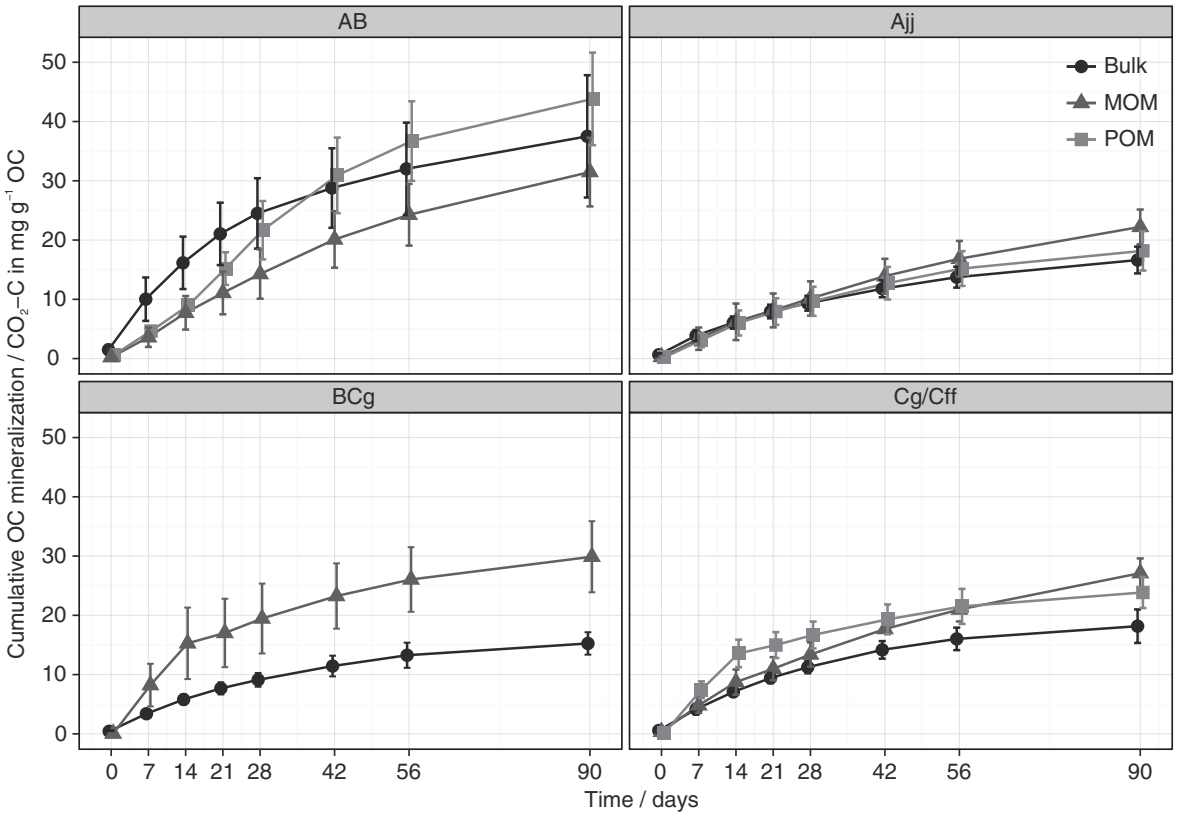

Figure 9 Cumulative OC mineralization of mineral-associated (MOM) and particulate OM (POM) and bulk soil material (bulk). Whiskers are sometimes smaller than symbols and show the SD. Sample numbers (*N*) of bulk soil and MOM including replicates were: AB, $N = 9$; Ajj, $N = 24$; BCg, $N = 12$; Cg/Cff, $N = 9$; and for the POM fraction: AB, $N = 3$; Ajj, $N = 24$; Cg/Cff, $N = 3$.

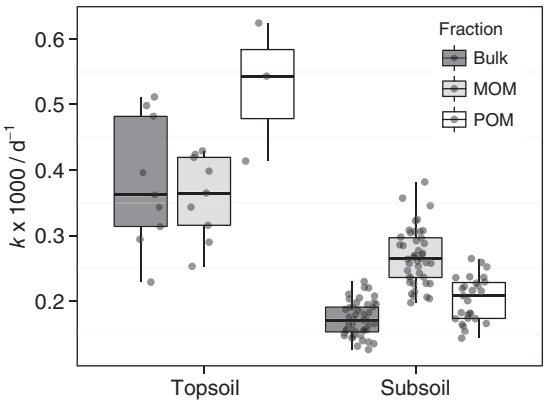

Figure 10 Observed first-order decay rate constants from 90-day incubation experiments for OM fractions and the bulk soil (*N* equals those in Figure 9).

OC was in a lower range than that from laboratory incubation studies with soil heavy density fractions or artificial mineral-organic associations (Table S7, File S1). Jagadamma *et al.* (2013) found only slight differences in the decomposability of POM and MOM from a Gelisol after 150 days incubation (about 10% of total OC mineralized), with the MOM fraction being mineralized faster than the POM fraction. In laboratory incubations, a stabilizing effect of the mineral phase on mineral-bound OM is often inferred from decomposition rates that are less than those for the respective unprotected OM that is not adsorbed or precipitated. For tundra sites in Alaska, Michaelson *et al.* (1998) reported that DOC, as a potential source of MOM, leached from thawing soil cores (pH 4.6 and 7.3) was primarily composed of polysaccharide-rich components and bioavailable, losing 34–46% of C in a 14-day incubation at 4°C. Hence, DOC from permafrost soils appears to be much more vulnerable to decomposition than our MOM fractions. The fact that the O-alkyl C:methoxyl C ratio of MOM was positively related to the mineralization rate constant agrees with the view that aromatic-rich dissolved OM is intrinsically more resistant to biodegradation than carbohydrate-rich OM and also interacts more strongly with minerals, resulting in less desorption and, therefore, mineralization (Kleber *et al.*, 2015). Gillespie *et al.* (2014) also found a larger mineralization potential for OM from Cryosol B horizons, which comprised more carbohydrate C relative to ketone C. However, they suggested that lignin-derived phenolics likewise represented a labile OM source. The negative relationship between decomposition rates and the Fe_p:Fe_o ratio ($R^2 = 0.41$; $P < 0.01$; $N = 18$) implies that organically complexed Fe rather than the whole pedogenic Fe pool reduces the bioavailability of mineral-bound OM, probably by minimizing the solubility in Fe-OM co-precipitates.

The extremely slow decomposition of POM in the subsoil is surprising and probably occurs because the easily available C necessary to stimulate microbial breakdown had already been leached or consumed by the decomposers during its longer residence time (Figure 6). A lack of easily available C (and N) has been demonstrated in priming experiments, particularly for the subsoil horizons (Wild *et al.*, 2014). The poor bioavailability of MOM, which is comparable to that in other climates (Table S7, File S1), is surprising given the less optimal soil conditions for the formation of stable mineral-organic associations in permafrost soils. The pH value (pH 5–8; Table 2), which is close to the point of zero charge of Fe and Al oxides (pH 7–9), theoretically diminishes the effective sorption and stabilization of OM on the surface of these minerals or clay edges. The aquic conditions (Vodyanitskii *et al.*, 2008) accompanied by reductive dissolution of Fe(III) oxides in permafrost soils should also not favour the effective stabilization of OM by Fe oxides. The restricted decomposability of MOM even under optimal conditions, however, in addition explains the formation of large MOM stocks and small ^{14}C activities (between 0.82 and 0.35 pMC) in the soil that we studied.

Conclusions

This study confirms that OM in permafrost-affected tundra soils is not 'inactivated' but microbially transformed over thousands of years under unfavourable conditions, leading to a large fraction of ^{13}C and ^{15}N-enriched OM associated with minerals and to an enrichment of alkyl and aromatic compounds with soil depth. The build-up of the large MOM pool ($54 \pm 16\%$ of the total soil OC) in these permafrost soils is the result of multiple processes, including the adsorption of DOC or microbial remnants to clay minerals and Al and Fe oxides (with a stronger emphasis on Al phases) as well as the co-precipitation of DOC, which is a yet under-rated mechanism in permafrost soils. Although the majority of MOM was not readily available under the optimal temperature and nutrient conditions, it contains a biologically active OM pool ($< 5\%$) that can be used by microorganisms. The finding of less bioavailable POM in the subsoil than in the topsoil is indicative of the limited energy-rich C sources required for microbial decomposition in deep soil horizons. An increasing input of easily available OM has been claimed as being responsible for stimulation of microbial activity in mineral subsoil in a 20-year soil warming experiment (Sistla *et al.*, 2013) and recent priming experiments (Wild *et al.*, 2014). For our results, this suggests that a part of this activity results from the use of mineral-bound OM under the 'neutral' soil conditions. We assume that as well as freezing and water-logging, stabilization of OM by associations with minerals is one key mechanism for OM conservation in arctic permafrost soils, which might become increasingly important with a future rise in soil temperatures and drier conditions. Given the abundance of a bioactive OC fraction, future research should not ignore the function and fate of mineral-organic associations, which hold the dominating OC pool in mineral horizons of permafrost soils.

Supporting Information

The following supporting information is available in the online version of this article:

File S1. Properties and bioavailability of particulate and mineral-associated organic matter in Arctic permafrost soils, Lower Kolyma Region, Russia.

Acknowledgements

Financial support was provided by the German Federal Ministry of Education and Research (03F0616A) within the ERANET EUROPOLAR project CryoCARB. OS and GG appreciate funding from the Russian Ministry of Education and Science (No. 14.B25.31.0031), and AR acknowledges the financial support of the Austrian Science Fund (FWF - I370-B17). NG appreciates the financial support of the Evangelisches Studienwerk Villigst. Thanks to all members of the CryoCARB project for the incredible team spirit. We are grateful to Roger-Michael Klatt and Pieter Wiese for laboratory assistance.

References

Alekseev, A., Alekseeva, T., Ostroumov, V., Siegert, C. & Gradusov, B. 2003. Mineral transformations in permafrost-affected soils, North Kolyma lowland, Russia. *Soil Science Society of America Journal*, **67**, 596–605.

Bonanomi, G., Incerti, G., Giannino, F., Mingo, A., Lanzotti, V. & Mazzoleni, S. 2013. Litter quality assessed by solid state ^{13}C NMR spectroscopy predicts decay rate better than C/N and Lignin/N ratios. *Soil Biology & Biochemistry*, **56**, 40–48.

Borden, P.W., Ping, C.-L., McCarthy, P.J. & Naidu, S. 2010. Clay mineralogy in Arctic tundra Gelisols, Northern Alaska. *Soil Science Society of America Journal*, **74**, 580–592.

DIN ISO 11277 2002. DIN ISO 11277. *Soil Quality – Determination of Particle Size Distribution in Mineral Soil Material – Method by Sieving and Sedimentation*. Deutsches Institut für Normung e.V., Berlin.

Fountain, A.G., Campbell, J.L., Schuur, E.A.G., Stammerjohn, S.E., Williams, M.W. & Ducklow, H.W. 2012. The disappearing cryosphere: impacts and ecosystem responses to rapid cryosphere loss. *BioScience*, **62**, 405–415.

Gentsch, N., Mikutta, R., Shibistova, O., Wild, B., Schnecker, J., Richter, A. *et al.* 2015. Storage and transformation of organic matter fractions in cryoturbated permafrost soils across the Siberian Arctic. *Biogeosciences Discussions*, **12**, 1–47.

Gerin, P.A., Genet, M.J., Herbillon, A.J. & Delvaux, B. 2003. Surface analysis of soil material by X-ray photoelectron spectroscopy. *European Journal of Soil Science*, **54**, 589–604.

Gillespie, A.W., Sanei, H., Diochon, A., Ellert, B.H., Regier, T.Z., Chevrier, D. *et al.* 2014. Perennially and annually frozen soil carbon differ in their susceptibility to decomposition: analysis of Subarctic earth hummocks by bioassay, XANES and pyrolysis. *Soil Biology & Biochemistry*, **68**, 106–116.

Gittel, A., Bárta, J., Kohoutová, I., Mikutta, R., Owens, S., Gilbert, J. *et al.* 2014. Distinct microbial communities associated with buried soils in the Siberian tundra. *The ISME Journal*, **8**, 841–853.

Gundelwein, A., Müller-Lupp, T., Sommerkorn, M., Haupt, E.T.K., Pfeiffer, E.-M. & Wiechmann, H. 2007. Carbon in tundra soils in the Lake

Labaz region of arctic Siberia. *European Journal of Soil Science*, **58**, 1164–1174.

Harris, D., Horwáth, W.R. & van Kessel, C. 2001. Acid fumigation of soils to remove carbonates prior to total organic carbon or CARBON-13 isotopic analysis. *Soil Science Society of America Journal*, **65**, 1853–1856.

Hartley, I.P., Garnett, M.H., Sommerkorn, M., Hopkins, D.W., Fletcher, B.J., Sloan, V.L. *et al.* 2012. A potential loss of carbon associated with greater plant growth in the European Arctic. *Nature Climate Change*, **2**, 875–879.

Höfle, S., Rethemeyer, J., Mueller, C.W. & John, S. 2013. Organic matter composition and stabilization in a polygonal tundra soil of the Lena Delta. *Biogeosciences*, **10**, 3145–3158.

IUSS Working Group WRB 2014. *World Reference Base for Soil Resources 2014. International Soil Classification System for Naming Soils and Creating Legends for Soil Maps*. Food and Agriculture Organization, Rome.

Jagadamma, S., Steinweg, J.M., Mayes, M.A., Wang, G. & Post, W.M. 2013. Decomposition of added and native organic carbon from physically separated fractions of diverse soils. *Biology & Fertility of Soils*, **50**, 1–9.

Kaiser, C., Meyer, H., Biasi, C., Rusalimova, O., Barsukov, P. & Richter, A. 2007. Conservation of soil organic matter through cryoturbation in arctic soils in Siberia. *Journal of Geophysical Research*, **112**, 9–17.

Kleber, M., Eusterhues, K., Keiluweit, M., Mikutta, C., Mikutta, R. & Nico, P.S. 2015. Mineral–organic associations: formation, properties, and relevance in soil environments. *Advances in Agronomy*, **130**, 1–140.

Lipson, D.A., Zona, D., Raab, T.K., Bozzolo, F., Mauritz, M. & Oechel, W.C. 2012. Water-table height and microtopography control biogeochemical cycling in an Arctic coastal tundra ecosystem. *Biogeosciences*, **9**, 577–591.

Michaelson, G.J., Ping, C.L., Kling, G.W. & Hobbie, J.E. 1998. The character and bioactivity of dissolved organic matter at thaw and in the spring runoff waters of the arctic tundra North Slope, Alaska. *Journal of Geophysical Research, [Atmospheres]*, **103**, 28939–28946.

Mikutta, R., Mikutta, C., Kalbitz, K., Scheel, T., Kaiser, K. & Jahn, R. 2007. Biodegradation of forest floor organic matter bound to minerals via different binding mechanisms. *Geochimica et Cosmochimica Acta*, **71**, 2569–2590.

Mikutta, R., Lorenz, D., Guggenberger, G., Haumaier, L. & Freund, A. 2014. Properties and reactivity of Fe-organic matter associations formed by coprecipitation versus adsorption: clues from arsenate batch adsorption. *Geochimica et Cosmochimica Acta*, **144**, 258–276.

Nadelhoffer, K., Shaver, G., Fry, B., Giblin, A., Johnson, L. & McKane, R. 1996. ^{15}N natural abundances and N use by tundra plants. *Oecologia*, **107**, 386–394.

Nowinski, N., Taneva, L., Trumbore, S. & Welker, J. 2010. Decomposition of old organic matter as a result of deeper active layers in a snow depth manipulation experiment. *Oecologia*, **163**, 785–792.

Ostroumov, V. 2004. Physico-chemical processes in cryogenic soils. In: *Cryosols* (ed J.M. Kimble), pp. 347–364. Springer, Berlin, Heidelberg.

Pansu, M. & Gautheyrou, J. 2006. *Handbook of Soil Analysis Mineralogical, Organic and Inorganic Methods*. Springer, Berlin.

Ping, C.L., Jastrow, J.D., Jorgenson, M.T., Michaelson, G.J. & Shur, Y.L. 2015. Permafrost soils and carbon cycling. *Soil*, **1**, 147–171.

Schädel, C., Schuur, E.A.G., Bracho, R., Elberling, B., Knoblauch, C., Lee, H. *et al.* 2013. Circumpolar assessment of permafrost C quality and its vulnerability over time using long-term incubation data. *Global Change Biology*, **20**, 641–652.

Schnecker, J., Wild, B., Hofhansl, F., Eloy Alves, R.J., Barta, J., Capek, P. *et al.* 2014. Effects of soil organic matter properties and microbial community composition on enzyme activities in cryoturbated arctic soils. *PLoS One*, **9**, e94076.

Schrumpf, M., Kaiser, K., Guggenberger, G., Persson, T., Kögel-Knabner, I. & Schulze, E.-D. 2013. Storage and stability of organic carbon in soils as related to depth, occlusion within aggregates, and attachment to minerals. *Biogeosciences*, **10**, 1675–1691.

Sistla, S.A., Moore, J.C., Simpson, R.T., Gough, L., Shaver, G.R. & Schimel, J.P. 2013. Long-term warming restructures Arctic tundra without changing net soil carbon storage. *Nature*, **497**, 615–618.

Soil Survey Staff 2010. *Keys to Soil Taxonomy*, 11th edn. United States Department of Agriculture-Natural Resources Conservation Service, Washington.

Stuiver, M. & Polach, H.A. 1977. Discussion; reporting of C-14 data. *Radiocarbon*, **19**, 355–363.

Tipping, E., Rey-Castro, C., Bryan, S.E. & Hamilton-Taylor, J. 2002. Al(III) and Fe(III) binding by humic substances in freshwaters, and implications for trace metal speciation. *Geochimica et Cosmochimica Acta*, **66**, 3211–3224.

Vodyanitskii, Y.N., Mergelov, N.S. & Goryachkin, S.V. 2008. Diagnostics of gleyzation upon a low content of iron oxides (using the example of tundra soils in the Kolyma Lowland). *Eurasian Soil Science*, **41**, 231–248.

Vonk, J.E., Mann, P.J., Davydov, S., Davydova, A., Spencer, R.G.M., Schade, J. *et al.* 2013. High biolability of ancient permafrost carbon upon thaw. *Geophysical Research Letters*, **40**, 2689–2693.

Walker, D.A., Raynolds, M.K., Daniëls, F.J.A., Einarsson, E., Elvebakk, A., Gould, W.A. *et al.* 2005. The circumpolar arctic vegetation map. *Journal of Vegetation Science*, **16**, 267–282.

Wild, B., Schnecker, J., Bárta, J., Čapek, P., Guggenberger, G., Hofhansl, F. *et al.* 2013. Nitrogen dynamics in Turbic Cryosols from Siberia and Greenland. *Soil Biology & Biochemistry*, **67**, 85–93.

Wild, B., Schnecker, J., Alves, R.J.E., Barsukov, P., Bárta, J., Čapek, P. *et al.* 2014. Input of easily available organic C and N stimulates microbial decomposition of soil organic matter in arctic permafrost soil. *Soil Biology & Biochemistry*, **75**, 143–151.

Ziadi, N. & Tran, T.S. 2006. Mehlich 3-extractable elements. In: *Soil Sampling and Methods of Analysis*, 2nd edn (eds B.J. Carter & E.G. Gregorich), pp. 107–114. CRC Press, Boca Raton, FL.